$Nb_4Pd_{0.5}ZSb_2$ (Z = Cr, Fe, Co, Ni, Si): The First Ordered Quaternary Variants of the W_5Si_3-Type Structure

Meitian Wang, William C. Sheets, Robert McDonald,† and Arthur Mar*

Department of Chemistry, University of Alberta, Edmonton, Alberta, Canada T6G 2G2

Received April 26, 2001

A family of quaternary (or pseudoquaternary) antimonides $Nb_4Pd_{0.5}ZSb_2$ (Z = Cr, Fe, Co, Ni, Si) containing up to three transition metals in an ordered arrangement has been prepared by reactions of the elements. These antimonides are isostructural, crystallizing as substitutional variants of the W_5Si_3-type structure (tetragonal, space group D_{4h}^{18}-*I*4/*mcm*, *Z* = 4) with unit cell parameters *a* = 10.4407(3) Å and *c* = 5.0020(2) Å for $Nb_4Pd_{0.5}Cr_{0.28(3)}Si_{0.72}Sb_2$, *a* = 10.4825(6) Å and *c* = 4.9543(3) Å for $Nb_4Pd_{0.5}FeSb_2$, *a* = 10.4603(5) Å and *c* = 4.9457(3) Å for $Nb_4Pd_{0.5}CoSb_2$, *a* = 10.4332(7) Å and *c* = 4.9649(3) Å for $Nb_4Pd_{0.5}Ni_{0.78(1)}Sb_2$, and *a* = 10.3895(10) Å and *c* = 4.9634(4) Å for $Nb_4Pd_{0.5}SiSb_2$. They are distinguished by the filling of interstitial Z atoms into the centers of Nb_8 square antiprismatic clusters that are linked by $PdSb_4$ tetrahedra. The Nb_8 square antiprisms share opposite square faces to form one-dimensional chains along the *c* axis so that Z−Z bonding distances of ∼2.5 Å result. Extended Hückel band structure calculations were carried out to interpret the homo- and heteroatomic metal−metal interactions in the structure. The resistivity of one member, $Nb_4Pd_{0.5}SiSb_2$, was measured, indicating metallic behavior.

Introduction

The early transition metals, having few valence electrons in relatively expanded d orbitals, form clusters through multicenter metal−metal bonding in a variety of molecular species and extended structures.[1] Interstitial atoms are often contained within these electron-deficient polyhedra, stabilizing them by supplementing the weak metal−metal bonds with strong metal−interstitial bonds.[1,2] The most frequently observed cluster types are octahedra (or trigonal antiprisms) (**1**), trigonal prisms with capping atoms on one or more quadrilateral faces (**2**), and square antiprisms (**3**). These polyhedra can be centered by a gamut of interstitial atoms, including first-row transition metals, second- and third-row main-group elements, and hydrogen.

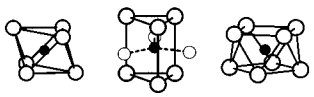

In the past two decades, early transition metal rich halides and chalcogenides have been the most exhaustively studied class of cluster compounds with extended structures. In the halides, cluster **1** is the usual basic building block observed,[3] whereas in the chalcogenides, cluster **2** is more prevalent and clusters **1** and **3** are less commonly found.[4,5] In contrast, much less is known about the existence of clusters among early transition metal rich pnictides. All three clusters have been identified thus far in the structures of these pnictides. For example, Zr_5NiSb_3 (Ti_5Ga_4-type) contains cluster **1**,[6] Zr_6FeSb_2 (Zr_6CoAl_2-type) contains cluster **2**,[7] and V_4SiSb_2 contains cluster **3**.[8] These clusters can be further condensed by sharing their corners, edges, or faces to give a rich structural chemistry.

The V_4SiSb_2 structure is particularly intriguing in featuring apparently empty channels surrounded by the pnicogen atoms. A recent band structure calculation on the isostructural bismuthides Ti_4ZBi_2 (Z = Cr, Mn, Fe, Co, Ni)[9] implied that electrophilic species could be feasibly intercalated into the tetrahedral voids of these channels, interacting with the lone pairs of the surrounding pnicogen atoms.[10] We were thus interested in the possibility of preparing quaternary early transition metal rich pnictide cluster compounds in which these voids are filled by guest atoms while accommodating a wide variety of interstitial atoms Z (Si as well as first-row transition metals) within clusters of type **3**.

Extending our systematic studies of ternary transition metal rich pnictides, in which we have discovered the compounds $M_3Pd_4P_3$ (M = Zr, Hf),[11] $Nb_5Pd_4P_4$,[11] $M_3Ni_3Sb_4$ (M = Zr, Hf),[12] $Zr_3Pt_3Sb_4$,[12] and $Nb_{28}Ni_{33.5}Sb_{12.5}$,[13] we report here several members of a new family of quaternary (or pseudoquaternary) transition metal rich antimonides $Nb_4Pd_{0.5}ZSb_2$ (Z = Cr, Fe, Co, Ni, Si). They represent the first examples of a filled V_4SiSb_2-type structure, or a quaternary *ordered* substitutional variant of the W_5Si_3-type structure.[14]

* To whom correspondence should be addressed. Telephone: (780) 492-5592. Fax: (780) 492-8231. E-mail: arthur.mar@ualberta.ca.
† Faculty Service Officer, X-ray Crystallography Laboratory.

(1) (a) *Clusters and Colloids*; Schmid, G., Ed.; Wiley-VCH: Weinheim, 1994. (b) Simon, A. *Angew. Chem., Int. Ed. Engl.* **1988**, *27*, 159.
(2) Corbett, J. D.; Garcia, E.; Kwon, Y.-U.; Guloy, A. *Pure Appl. Chem.* **1990**, *62*, 103.
(3) Corbett, J. D. *J. Alloys Compd.* **1995**, *229*, 10.
(4) Hughbanks, T. *J. Alloys Compd.* **1995**, *229*, 40.
(5) Tremel, W.; Kleinke, H.; Derstroff, V.; Reisner, C. *J. Alloys Compd.* **1995**, *219*, 73.
(6) Garcia, E.; Corbett, J. D. *Inorg. Chem.* **1990**, *29*, 3274.
(7) Melnyk, G.; Bauer, E.; Rogl, P.; Skolozdra, R.; Seidl, E. *J. Alloys Compd.* **2000**, *296*, 235.
(8) Wollesen, P.; Jeitschko, W. *J. Alloys Compd.* **1996**, *243*, 67.
(9) Richter, C. G.; Jeitschko, W.; Künnen, B.; Gerdes, M. H. *J. Solid State Chem.* **1997**, *133*, 400.
(10) Rytz, R.; Hoffmann, R. *Inorg. Chem.* **1999**, *38*, 1609.
(11) Wang, M.; McDonald, R.; Mar, A. *Inorg. Chem.* **2000**, *39*, 4936.
(12) Wang, M.; McDonald, R.; Mar, A. *Inorg. Chem.* **1999**, *38*, 3435.
(13) Wang, M.; Mar, A. *J. Solid State Chem.*, in press.

10.1021/ic010441z CCC: $20.00
Published on Web 08/23/2001

Table 1. Crystallographic Data for $Nb_4Pd_{0.5}ZSb_2$ (Z = Cr, Fe, Co, Ni, Si)

	$Nb_4Pd_{0.5}Cr_{0.28}Si_{0.72}Sb_2$	$Nb_4Pd_{0.5}FeSb_2$	$Nb_4Pd_{0.5}CoSb_2$	$Nb_4Pd_{0.5}Ni_{0.78}Sb_2$	$Nb_4Pd_{0.5}SiSb_2$
formula mass (amu)	703.11	724.19	727.27	713.88	696.43
space group	D_{4h}^{18}-*I*4/*mcm* (No. 140)	D_{4h}^{18}-*I*4/*mcm* (No. 140)	D_{4h}^{18}-*I*4/*mcm* (No. 140)	D_{4h}^{18}-*I*4/*mcm* (No. 140)	D_{4h}^{18}-*I*4/*mcm* (No. 140)
a (Å)[a]	10.4407(3)	10.4825(6)	10.4603(5)	10.4332(7)	10.3895(10)
c (Å)[a]	5.0020(2)	4.9543(3)	4.9457(3)	4.9649(3)	4.9634(4)
V (Å^3)	545.26(3)	544.39(6)	541.15(5)	540.44(6)	535.76(8)
Z	4	4	4	4	4
T (°C)	22	22	22	22	22
λ (Å)	0.71073	0.71073	0.71073	0.71073	0.71073
ρ_{calcd} (g cm^{-3})	8.564	8.836	8.927	8.773	8.634
μ(Mo Kα) (cm^{-1})	200.28	219.18	224.34	221.20	198.97
$R(F)$ for $F_o^2 > 2\sigma(F_o^2)$[b]	0.031	0.035	0.030	0.034	0.040
$R_w(F_o^2)$[c]	0.075	0.086	0.077	0.075	0.091

[a] Obtained from a refinement constrained so that $a = b$ and $\alpha = \beta = \gamma = 90°$. [b] $R(F) = \sum||F_o| - |F_c||/\sum|F_o|$. [c] $R_w(F_o^2) = [\sum[w(F_o^2 - F_c^2)^2]/\sum wF_o^4]^{1/2}$; $w^{-1} = [\sigma^2(F_o^2) + (ap)^2 + bp]$ where $p = [\max(F_o^2,0) + 2F_c^2]/3$. For $Nb_4Pd_{0.5}Cr_{0.28}Si_{0.72}Sb_2$, $a = 0.0302$ and $b = 23.7359$; for $Nb_4Pd_{0.5}FeSb_2$, $a = 0.0437$ and $b = 17.0051$; for $Nb_4Pd_{0.5}CoSb_2$, $a = 0.0439$ and $b = 5.3596$; for $Nb_4Pd_{0.5}Ni_{0.78}Sb_2$, $a = 0.0383$ and $b = 0.0000$; for $Nb_4Pd_{0.5}SiSb_2$, $a = 0.0441$ and $b = 0.0000$.

Experimental Section

Synthesis. Reactants used were the elemental powders (Nb, 99.8%, Cerac; Pd, 99.95%, Alfa-Aesar; Cr, 99.95%, Cerac; Fe, 99.9%, Cerac; Co, 99.8%, Cerac; Ni, 99.9%, Cerac; Si, 99.96%, Cerac; Sb, 99.995%, Aldrich). In the course of investigating the ternary Nb−Pd−Sb system, $Nb_4Pd_{0.5}SiSb_2$ was first identified in a direct reaction of Nb, Pd, and Sb in a 1:1:1 molar ratio (total weight 0.25 g) placed in an evacuated fused-silica tube. The reactants were heated at 1100 °C for 12 h and then at 1000 °C for 4 days. The silica tube served as the source of Si in the products. EDX (energy-dispersive X-ray) analysis of several crystals from the above reaction on a Hitachi S2700 scanning electron microscope suggested an approximate atomic composition of 50% Nb, 8% Pd, 12% Si, and 30% Sb (with typical uncertainties of 1−2%). On this basis, a mixture of Nb, Pd, Si, and Sb in a 5:1:1:3 ratio was reacted at 1000 °C for 3 days. A needle-shaped crystal from this reaction was selected for the structure determination, which revealed the correct composition to be $Nb_4Pd_{0.5}SiSb_2$ (53% Nb, 7% Pd, 13% Si, 27% Sb). A stoichiometric reaction of the elements in the correct ratio at 1000 °C for 3 days afforded a quantitative yield of $Nb_4Pd_{0.5}SiSb_2$, as revealed by X-ray powder diffraction patterns obtained on an Enraf-Nonius FR552 Guinier camera (Cu Kα_1 radiation).

Since Si can be replaced by some first-row transition metals as an interstitial atom in other cluster structures such as Ta_4ZTe_4,[15] substitution of the Si atoms in $Nb_4Pd_{0.5}SiSb_2$ by Fe was first attempted. Two direct reactions of Nb, Pd, Fe, and Sb in 5:1:1:3 and 4:0.5:1:2 ratios at 1000 °C for 3 days were carried out. The products in both reactions contained more than 50% $Nb_4Pd_{0.5}FeSb_2$, as well as the phases NbFeSb and Nb_3Sb, as determined by X-ray powder diffraction patterns. EDX analyses on several needle-shaped crystals confirmed the presence of all four elements in the atomic proportions 49% Nb, 9% Pd, 12% Fe, and 30% Sb. One crystal from the first reaction (5:1:1:3 ratio) was chosen for the structure determination.

Subsequently, reactions of Nb, Pd, Z, and Sb in both 5:1:1:3 and 4:0.5:1:2 ratios were carried out for Z = Cr−Zn. For Z = Co and Ni, the quaternary compounds were obtained as needle-shaped crystals, as verified by EDX analyses which indicated compositions of 49% Nb, 9% Pd, 13% Co, 29% Sb (average of five crystals) and 53% Nb, 7% Pd, 10% Ni, 31% Sb (average of six crystals), respectively. For Z = Cr, incorporation of Si from the silica tube occurred to give crystals containing *five* elements present in the proportions 49% Nb, 7% Pd, 6% Cr, 9% Si, 29% Sb (average of five crystals). We have been unable to prepare an all-Cr compound free from Si incorporation. When the reaction was repeated in an alumina crucible jacketed by a silica tube, the desired phase was not formed, but rather the product consisted predominantly of binary phases such as Nb_3Sb. For Z = Mn, Cu, and Zn, no quaternary phases were obtained under any of the synthetic conditions described above.

Structure Determination. All crystals were screened by EDX analysis and Weissenberg photography. Intensity data were collected at room temperature (22 °C) on a Bruker Platform/SMART 1000 CCD diffractometer using ω scans (0.2°) in the range $5.52° \le 2\theta$ (Mo Kα) $\le 65.12°$ for $Nb_4Pd_{0.5}Cr_{0.28}Si_{0.72}Sb_2$, $5.50° \le 2\theta$ (Mo Kα) $\le 65.10°$ for $Nb_4Pd_{0.5}FeSb_2$, $5.50° \le 2\theta$ (Mo Kα) $\le 65.14°$ for $Nb_4Pd_{0.5}CoSb_2$, $5.52° \le 2\theta$ (Mo Kα) $\le 65.18°$ for $Nb_4Pd_{0.5}Ni_{0.78}Sb_2$, and $5.54° \le 2\theta$ (Mo Kα) $\le 52.66°$ for $Nb_4Pd_{0.5}SiSb_2$. Crystal data and further details of the data collections are given in Table 1. All calculations were carried out with use of the SHELXTL (version 5.1) package.[16] Conventional atomic scattering factors and anomalous dispersion corrections were used.[17] Intensity data were processed, and face-indexed numerical absorption corrections were applied in XPREP.

The five compounds are isostructural. Weissenberg photographs revealed tetragonal symmetry in all cases. The Laue symmetry 4/*mmm* and the systematic extinctions suggested space groups *I*4/*mcm*, *I*4*cm*, and $I\bar{4}c2$. The centrosymmetric space group *I*4/*mcm* (No. 140) was chosen on the basis of the successful structure solution and refinement. The positions of all atoms were found by direct methods. In the early stages of refinement, the displacement parameter of the Pd site was unusually large, implying that it is partially occupied. For example, when refined, the occupancy of the Pd site converged to 56(2)% in the Fe-containing and 58(2)% in the Si-containing compound. In all compounds, the closest separation between Pd sites is ~2.47−2.50 Å, which would be unusually short for a Pd−Pd bond (cf. 2.56 Å from the sum of two Pauling single-bond metallic radii of Pd[18] or 2.75 Å for the Pd−Pd distance in elemental Pd[19]). Although the possibility that these short Pd−Pd contacts genuinely exist cannot be excluded, we chose the simplest interpretation in which they are precluded by setting the Pd occupancy to 50%.

The subsequent refinements for $Nb_4Pd_{0.5}FeSb_2$, $Nb_4Pd_{0.5}CoSb_2$, and $Nb_4Pd_{0.5}SiSb_2$ proceeded in a straightforward manner, with full occupancies of all sites other than that of Pd. For the pseudoquaternary compound $Nb_4Pd_{0.5}(Cr_xSi_{1-x})Sb_2$, the Z site was modeled to accommodate a disorder of Cr and Si atoms in proportions that sum to full occupancy. With this constraint, the occupancies refined to 28(3)% Cr and 72% Si. For the Ni-containing compound, the displacement parameter of the Z site remained somewhat large, suggesting a substoichiometry in Ni. Consistent with the lower than expected content of Ni found in the EDX analysis, the occupancy of this site converged to 78(1)% Ni when allowed to refine.

The final refinements for all compounds led to generally well-behaved anisotropic displacement parameters. The thermal ellipsoids

(14) Aronsson, B. *Acta Chem. Scand.* **1955**, *9*, 1107.
(15) Badding, M. E.; DiSalvo, F. J. *Inorg. Chem.* **1990**, *29*, 3952.
(16) Sheldrick, G. M. *SHELXTL*, version 5.1; Bruker Analytical X-ray Systems, Inc.: Madison, WI, 1997.
(17) *International Tables for X-ray Crystallography*; Wilson, A. J. C., Ed.; Kluwer: Dordrecht, The Netherlands, 1992; Vol. C.
(18) Pauling, L. *The Nature of the Chemical Bond*, 3rd ed.; Cornell University Press: Ithaca, NY, 1960.
(19) Donohue, J. *The Structures of the Elements*; Wiley: New York, 1974.

Table 2. Positional and Equivalent Isotropic Displacement Parameters for $Nb_4Pd_{0.5}ZSb_2$ (Z = Cr, Fe, Co, Ni, Si)

atom	Wyckoff position	*x*	*y*	*z*	U_{eq} (Å^2)[a]
		$Nb_4Pd_{0.5}Cr_{0.28(3)}Si_{0.72}Sb_2$			
Nb	16*k*	0.08161(6)	0.20758(6)	0	0.0066(2)
Pd[b]	4*b*	0	1/2	1/4	0.0100(4)
Z[c]	4*a*	0	0	1/4	0.0083(10)
Sb	8*h*	0.15137(5)	0.65137(5)	0	0.0149(3)
		$Nb_4Pd_{0.5}FeSb_2$			
Nb	16*k*	0.08130(7)	0.20657(7)	0	0.0066(3)
Pd[b]	4*b*	0	1/2	1/4	0.0082(5)
Fe	4*a*	0	0	1/4	0.0104(5)
Sb	8*h*	0.15123(6)	0.65123(6)	0	0.0138(3)
		$Nb_4Pd_{0.5}CoSb_2$			
Nb	16*k*	0.08072(6)	0.20643(6)	0	0.0076(2)
Pd[b]	4*b*	0	1/2	1/4	0.0094(4)
Co	4*a*	0	0	1/4	0.0078(4)
Sb	8*h*	0.15145(5)	0.65145(5)	0	0.0148(3)
		$Nb_4Pd_{0.5}Ni_{0.78(1)}Sb_2$			
Nb	16*k*	0.08182(10)	0.20813(9)	0	0.0046(3)
Pd[b]	4*b*	0	1/2	1/4	0.0079(7)
Ni[d]	4*a*	0	0	1/4	0.0042(10)
Sb	8*h*	0.15079(7)	0.65079(7)	0	0.0120(3)
		$Nb_4Pd_{0.5}SiSb_2$			
Nb	16*k*	0.0811(2)	0.2073(2)	0	0.0080(7)
Pd[b]	4*b*	0	1/2	1/4	0.0067(15)
Si	4*a*	0	0	1/4	0.006(3)
Sb	8*h*	0.15241(14)	0.65241(14)	0	0.0136(8)

[a] U_{eq} is defined as one-third of the trace of the orthogonalized $\mathbf{U}_{ij}$ tensor. [b] 50% occupancy. [c] 28(3)% Cr and 72% Si. [d] 78(1)% occupancy.

of the Sb sites are somewhat elongated along the *c* axis, perhaps reflecting the tendency of the Sb atoms to be displaced either slightly above or below the mirror plane (*x*, *y*, 0) depending on whether a Pd atom locally occupies the site above or below. Indeed, the Sb atom can be refined with 50% occupancy at two split sites off the mirror plane. For example, in $Nb_4Pd_{0.5}FeSb_2$, the sites are displaced ~0.14 Å off the mirror plane. However, in other cases, the resolution of the split sites is sufficiently poor that correlation between the positional and displacement parameters renders the refinement unstable. We therefore opted to retain the Sb position on the mirror plane with the understanding that the elongation of the thermal ellipsoid is an artifact that results from averaging two closely spaced split sites. Satisfactory residuals (Table 1) and featureless difference electron maps ($\Delta\rho_{max}$ = 2.25 e$^-$ Å^{-3}, $\Delta\rho_{min}$ = −1.36 e$^-$ Å^{-3} for $Nb_4Pd_{0.5}Cr_{0.28(3)}Si_{0.72}Sb_2$; $\Delta\rho_{max}$ = 2.78 e$^-$ Å^{-3}, $\Delta\rho_{min}$ = −1.68 e$^-$ Å^{-3} for $Nb_4Pd_{0.5}FeSb_2$; $\Delta\rho_{max}$ = 2.20 e$^-$ Å^{-3}, $\Delta\rho_{min}$ = −2.04 e$^-$ Å^{-3} for $Nb_4Pd_{0.5}CoSb_2$; $\Delta\rho_{max}$ = 2.60 e$^-$ Å^{-3}, $\Delta\rho_{min}$ = −1.99 e$^-$ Å^{-3} for $Nb_4Pd_{0.5}Ni_{0.78(1)}Sb_2$; and $\Delta\rho_{max}$ = 2.18 e$^-$ Å^{-3}, $\Delta\rho_{min}$ = −2.71 e$^-$ Å^{-3} for $Nb_4Pd_{0.5}SiSb_2$) were obtained for all structures. The atomic positions were standardized with the program STRUCTURE TIDY.[20] Final values of the positional and displacement parameters are given in Table 2. Selected interatomic distances are listed in Table 3. Further data in the form of a CIF are available as Supporting Information, and final structural amplitudes are available from the authors.

Electrical Resistivity. A pressed pellet of $Nb_4Pd_{0.5}SiSb_2$ with dimensions of 0.53 × 0.30 × 0.05 cm was mounted in a four-probe configuration for an ac resistivity measurement between 2 and 300 K on a Quantum Design PPMS system equipped with an ac-transport controller (model 7100). A current of 0.1 mA and a frequency of 16 Hz were used. Measurements on the other members could not be performed owing to difficulties in preparing phase-pure material or single crystals of adequate size.

Band Structure. One-electron band structure calculations on $Nb_4Pd_{0.5}FeSb_2$ and $Nb_4Pd_{0.5}SiSb_2$ were performed with use of the EHMACC suite of programs.[21,22] The 50% Pd occupancy was modeled by alternately removing every second Pd atom within each $^1_\infty[Pd_{0.5}Sb_{4/2}]$ column. Extended Hückel parameters were taken from literature values and are listed in Table 4. Properties were extracted from the band structure using 128 *k* points in the irreducible portion of the Brillouin zone.

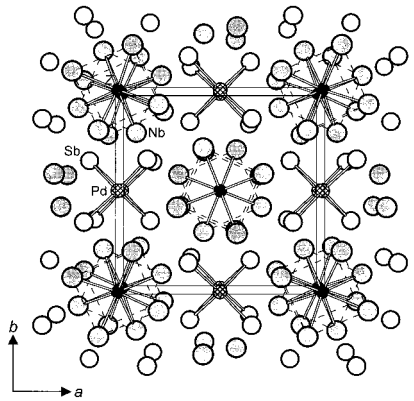

Figure 1. Structure of $Nb_4Pd_{0.5}ZSb_2$ (Z = Cr, Fe, Co, Ni, Si) viewed in projection down the *c* axis. The large lightly shaded circles are Nb atoms, the medium solid circles are Z atoms, the hatched circles are Pd atoms, and the open circles are Sb atoms.

Results and Discussion

Crystal Structure. The quaternary (or pseudoquaternary, in the case of $Nb_4Pd_{0.5}Cr_{0.28}Si_{0.72}Sb_2$) transition-metal antimonides $Nb_4Pd_{0.5}ZSb_2$ (Z = Cr, Fe, Co, Ni, Si) adopt a three-dimensional structure than can be described by linking one-dimensional $^1_\infty[Nb_{8/2}Z]$ and $^1_\infty[Pd_{0.5}Sb_{4/2}]$ columns together, as shown in a projection along the *c* axis in Figure 1.

In this view, it is easy to visualize the Nb_8 square antiprismatic clusters centered by interstitial Z atoms (**3**) whose 4-fold axis coincides with the *c* axis. The Nb−Z distances within the square antiprisms are ~2.63 Å and indicate strong interactions. For example, the Nb−Fe distance (2.6361(7) Å) in $Nb_4Pd_{0.5}FeSb_2$ falls within the range of those in the binary intermetallic μ-phase Nb_6Fe_7 (nearest neighbor Nb−Fe distances of 2.54−2.64 Å),[23] and the Nb−Si distance in $Nb_4Pd_{0.5}SiSb_2$ (2.624(2) Å) is comparable to those in binary niobium silicides (e.g., Nb−Si distance of 2.59 Å in Nb_5Si_3[24] or 2.62 Å in $NbSi_2$[25]). The Z-centered Nb_8 square antiprisms then share opposite square faces to form the one-dimensional $^1_\infty[Nb_{8/2}Z]$ columns that run along the *c* direction. The resulting Z−Z distances (e.g., 2.4772(1) Å for Fe−Fe; 2.4817(2) Å for Si−Si), which are equal to half the *c* parameter, are short (cf. 2.48 Å for Fe−Fe in elemental Fe; 2.35 Å for Si−Si in elemental Si),[19] but whether they are truly strongly bonding of their own accord or a mere consequence of a matrix effect will be discussed later.

In all compounds, the Pd atoms are coordinated in a tetrahedral fashion by four Sb neighbors. These tetrahedra then share opposite edges to form the one-dimensional $^1_\infty[Pd_{0.5}Sb_{4/2}]$ columns that also run along the *c* direction. The Pd sites have a 50% occupancy to avoid abnormally short Pd−Pd contacts (equal to the Z−Z distances), suggesting a local ordering of alternately empty and filled tetrahedral sites within a column. The $^1_\infty[Pd_{0.5}Sb_{4/2}]$ columns are far apart from each other, so the

(20) Gelato, L. M.; Parthé, E. *J. Appl. Crystallogr.* **1987**, *20*, 139.
(21) Whangbo, M.-H.; Hoffmann, R. *J. Am. Chem. Soc.* **1978**, *100*, 6093.
(22) Hoffmann, R. *Solids and Surfaces: A Chemist's View of Bonding in Extended Structures*; VCH Publishers: New York, 1988.
(23) Raman, A. *Z. Metallkd.* **1996**, *57*, 301.
(24) Parthé, E.; Lux, B.; Nowotny, H. *Monatsh. Chem.* **1955**, *86*, 859.
(25) Kubiak, R.; Horyń, R.; Broda, H.; Łukaszewicz, K. *Bull. Acad. Pol. Sci., Ser. Sci. Chim.* **1972**, *20*, 429.

Table 3. Selected Interatomic Distances (Å) for $Nb_4Pd_{0.5}ZSb_2$ (Z = Cr, Fe, Co, Ni, Si)

	$Nb_4Pd_{0.5}Cr_{0.28}Si_{0.72}Sb_2$	$Nb_4Pd_{0.5}FeSb_2$	$Nb_4Pd_{0.5}CoSb_2$	$Nb_4Pd_{0.5}Ni_{0.78}Sb_2$	$Nb_4Pd_{0.5}SiSb_2$
Nb−Z	2.6433(6) (×2)	2.6361(7) (×2)	2.6276(6) (×2)	2.6429(9) (×2)	2.624(2) (×2)
Nb−Sb	2.8435(7)	2.8571(8)	2.8474(7)	2.8384(10)	2.830(2)
	2.8490(10)	2.8632(11)	2.8600(9)	2.8531(13)	2.827(3)
	2.9924(4) (×2)	2.9826(5) (×2)	2.9786(4) (×2)	2.9744(6) (×2)	2.972(1) (×2)
Nb−Nb	3.0264(8) (×2)	3.0069(9) (×2)	2.9944(7) (×2)	3.0129(12) (×2)	3.000(3) (×2)
	3.1169(8) (×2)	3.0960(9) (×2)	3.0941(8) (×2)	3.1042(12) (×2)	3.098(3) (×2)
	3.1127(13)	3.1448(16)	3.1487(13)	3.099(2)	3.109(4)
	3.2934(9) (×2)	3.2909(11) (×2)	3.2789(9) (×2)	3.2997(14) (×2)	3.270(3) (×2)
Pd−Sb	2.5611(7) (×4)	2.5612(8) (×4)	2.5589(7) (×4)	2.5477(10) (×4)	2.560(2) (×4)
Z−Z	2.5010(1) (×2)	2.4772(1) (×2)	2.4728(1) (×2)	2.4824(1) (×2)	2.4817(2) (×2)

Table 4. Extended Hückel Parameters

atom	orbital	H_{ii} (eV)	ζ_{i1}	c_1	ζ_{i2}	c_2
Nb	5s	−9.04	1.89			
	5p	−5.13	1.85			
	4d	−9.94	4.08	0.6401	1.64	0.5516
Pd	5s	−7.51	2.19			
	5p	−3.86	2.15			
	4d	−12.53	5.98	0.55	2.61	0.67
Fe	4s	−8.40	1.90			
	4p	−5.00	1.90			
	3d	−12.2	5.35	0.5505	2.00	0.6815
Si	3s	−17.3	1.383			
	3p	−9.2	1.383			
Sb	5s	−18.8	2.323			
	5p	−11.7	1.999			

distribution of locally ordered columns would still be randomized within the *ab* plane. The observed Pd−Sb distances of ∼2.56 Å are shorter than the sum of Pauling single-bond radii, 2.688 Å,[18] or typical distances of 2.6−2.8 Å found in most binary palladium antimonides, although distances as short as 2.54 Å have been observed in Pd_8Sb_3.[26] As discussed in the structure determination section, the elongation of the thermal ellipsoids of the neighboring Sb atoms along the *c* axis may reflect slight distortions of the $PdSb_4$ tetrahedra that are averaged out in the partial occupancy model of the structure.

The $^1_\infty[Nb_{8/2}Z]$ and $^1_\infty[Pd_{0.5}Sb_{4/2}]$ columns are connected together by Nb−Sb bonds to complete the three-dimensional structure. The Nb−Sb bond distances of ∼2.84−2.98 Å are similar to those found in binary niobium antimonides such as $NbSb_2$[27] and Nb_5Sb_4[28] (2.73−2.97 Å). There is a short intercolumn Nb−Nb bond (e.g., 3.1448(16) Å in $Nb_4Pd_{0.5}FeSb_2$ or 3.109(4) Å in $Nb_4Pd_{0.5}SiSb_2$), whose magnitude is comparable to the intracolumn Nb−Nb distances, that also connects $^1_\infty[Nb_{8/2}Z]$ columns together. Both Nb and Sb atoms have rather unusual coordination environments. Each Nb atom has six Nb and two Z neighbors within a $^1_\infty[Nb_{8/2}Z]$ column, one Nb neighbor in the adjacent $^1_\infty[Nb_{8/2}Z]$ column, and four Sb neighbors located at one side of the coordination polyhedron, resulting in a coordination number (CN) of 13. Each Sb atom is surrounded by eight Nb atoms from two $[Nb_{8/2}Z]$ columns and by two Pd sites (one of which is empty if the 50% occupancy is taken into account), giving an average CN of 9.

Structural Relationships. One-dimensional columns of interstitially stabilized square-antiprismatic clusters $^1_\infty[M_{8/2}Z]$ (M = Nb, Ta) are found, albeit infrequently, in other structures related to $Nb_4Pd_{0.5}ZSb_2$, as shown in Figure 2. In the Ta_2Si-type structure,[29] the $^1_\infty[Ta_{8/2}Si]$ columns are connected to each other by sharing all corners (Figure 2a). Although this structure appears to be quite dense, the channels in the intercolumn region

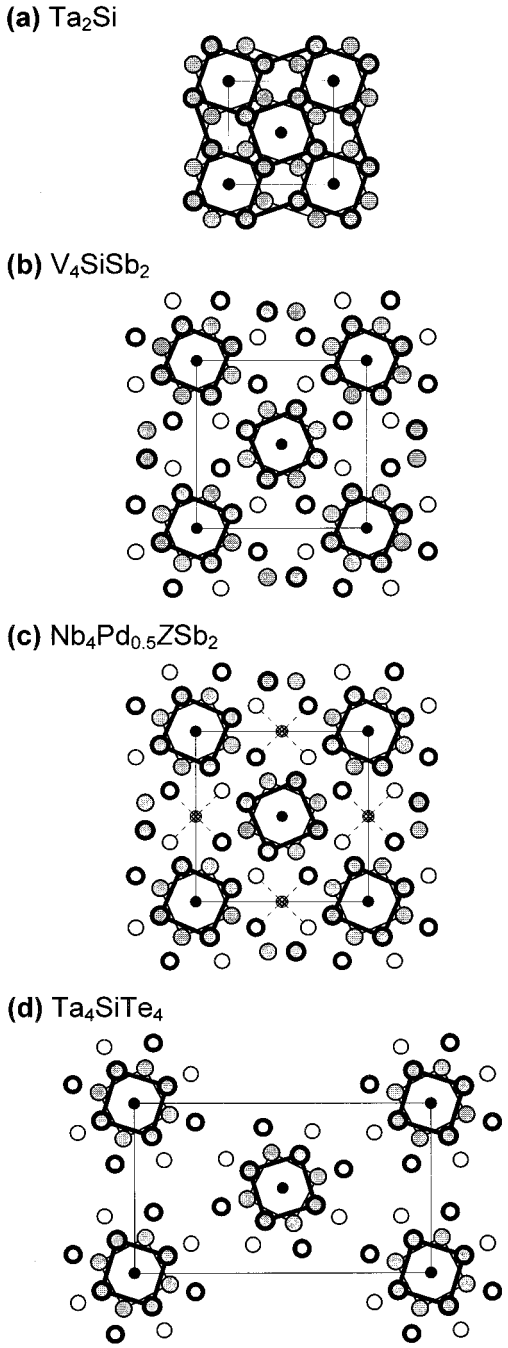

Figure 2. Comparison of the structures of (a) Ta_2Si, (b) V_4SiSb_2, (c) $Nb_4Pd_{0.5}ZSb_2$ (Z = Cr, Fe, Co, Ni, Si), and (d) Ta_4SiTe_4, in terms of one-dimensional columns of face-sharing Si- (or other Z-) filled square antiprisms, shown in projection down the *c* axis. Light and heavy lines indicate a displacement by $^1/_2$ the repeat along the projection axis.

(26) Wopersnow, W.; Schubert, K. *J. Less-Common Met.* **1976**, *48*, 79.
(27) (a) Furuseth, S.; Kjekshus, A. *Acta Crystallogr.* **1965**, *18*, 320. (b) Rehr, A.; Kauzlarich, S. M. *Acta Crystallogr., Sect. C: Cryst. Struct. Commun.* **1994**, *50*, 1177.
(28) Furuseth, S.; Kjekshus, A. *Acta Chem. Scand.* **1964**, *18*, 1180.
(29) Havinga, E. E.; Damsma, H.; Hokkeling, P. *J. Less-Common Met.* **1972**, *27*, 169.

are able to accommodate additional guest atoms within them, producing the TlSe-type structure.[30]

In contrast, the recently elucidated V_4SiSb_2-type structure contains $^1_\infty[V_{8/2}Si]$ columns that are capped along their periphery by Sb atoms to yield more open intercolumn regions (Figure 2b). Effectively, these Sb atoms are shared between $^1_\infty[V_{8/2}Si]$ columns and serve to link them together. The Sb atoms also form empty channels along ($^1/_2$, 0, *z*) and (0, $^1/_2$, *z*) consisting of tetrahedral sites spaced evenly along *c*. Electronic structure calculations confirmed the supposition that the empty channels in the isostructural bismuthides Ti_4ZBi_2 (Z = Cr, Mn, Fe, Co, Ni)[9] contain nonbonding electron density (lone pairs) from the surrounding pnicogen atoms and suggested the possibility of intercalating species such as Li^+ or Na^+ into these channels.[10] Perhaps somewhat astonishingly, the successful filling of these channels came about not from intercalation of Li or Na into the Ti_4ZBi_2 structure, as was proposed, but rather from intercalation (in a *Gedanken* manner) of Pd into a hypothetical "Nb_4ZSb_2" structure, to form the $Nb_4Pd_{0.5}ZSb_2$ compounds (Figure 2c). The observed Pd−Sb distances of ~2.56 Å in $Nb_4Pd_{0.5}ZSb_2$ are not that far off from the Li−Bi distance of 2.41 Å in a hypothetical "$LiTi_4FeBi_2$" compound.[10] Of course, the character of a Pd−Sb bond is quite different from that of a Li−Bi bond. We expect that achieving the electronic structure of $Nb_4Pd_{0.5}ZSb_2$ would entail a less severe redistribution of electron density in a hypothetical "Nb_4ZSb_2" compound than in a corresponding intercalation with Li.

The binary version of $Nb_4Pd_{0.5}ZSb_2$ is the well-known W_5Si_3-type structure.[14] This is a common intermetallic structure type (*I*4/*mcm*, *tI*32) adopted by nearly a hundred binary, pseudobinary, and ternary compounds.[31] Of the four different crystallographic sites (4*a*, 4*b*, 8*h*, and 16*k*) in the W_5Si_3-type structure, metals are usually located in 4*b* and 16*k*, and nonmetals or metalloids in 4*a* and 8*h*. For example, in the recently discovered ternary antimonides $Zr_5M_xSb_{3-x}$ (M = Fe, Co, Ni; $x \approx 0.5$)[32] and $Hf_{10}M_xSb_{6-x}$ (M = V, Cr, Mn, Fe, Co, Ni, Cu; $0.8 < x < 1.5$),[33] Zr or Hf atoms occupy sites 4*b* and 16*k*, Sb atoms occupy site 8*h*, and M and Sb atoms are approximately evenly distributed over site 4*a*. The compounds reported here, $Nb_4Pd_{0.5}ZSb_2$ (Z = Cr, Fe, Co, Ni, Si), are the first quaternary or pseudoquaternary variants of the W_5Si_3-type structure: Nb atoms occupy site 16*k*, Pd atoms site 4*b* (at 50%), Z atoms site 4*a*, and Sb atoms site 8*h*. It is remarkable that the structure of $Nb_4Pd_{0.5}ZSb_2$ can contain up to three different transition metals in an *ordered* arrangement.

Like the V_4SiSb_2 structure, the Ta_4SiTe_4 structure[15] contains empty channels formed between $^1_\infty[Ta_{8/2}Si]$ columns, which are further apart and capped by Te atoms (Figure 2d). The disparities in these two structures reflect the different chemistry of the pnicogens vs the chalcogens: whereas neighboring $^1_\infty[V_{8/2}Si]$ columns in V_4SiSb_2 are held strongly together by Sb atoms through V−Sb covalent bonds, the $^1_\infty[Ta_{8/2}Si]$ columns in Ta_4SiTe_4 are merely interacting between Te atoms through van der Waals forces, as frequently found in low-dimensional chalcogenides. Whether additional atoms can be inserted between these columns remains to be seen.

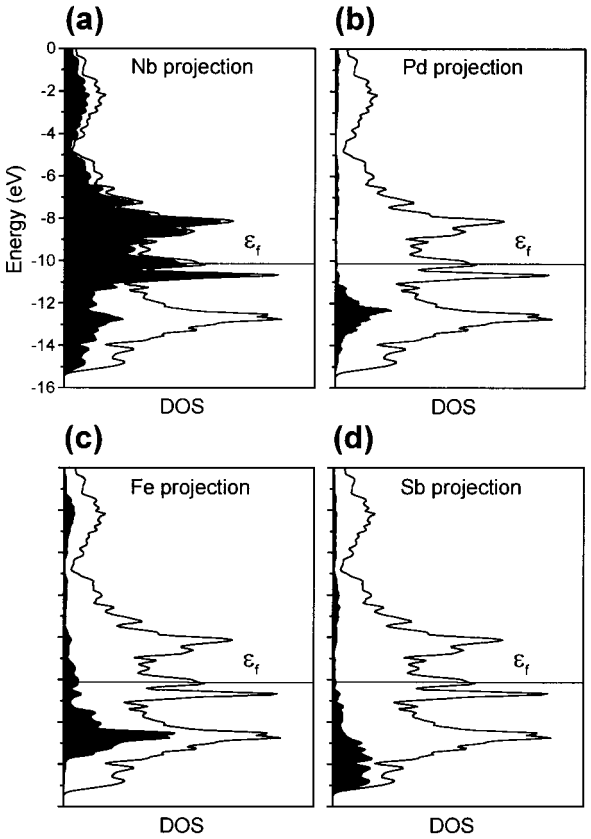

Figure 3. Contributions of (a) Nb, (b) Pd, (c) Fe, and (d) Sb (shaded regions) to the total density of states (DOS) (line) for $Nb_4Pd_{0.5}FeSb_2$. The Fermi level, ϵ_f, is at −10.08 eV.

All four structure types shown in Figure 2 have representatives in which Si is the interstitial Z atom centering the square antiprisms. The Z atom can also be replaced by first-row transition metals, but the range of substitution varies; viz., $Ta_2Si \rightarrow Nb_4CoSi$,[29,34] $V_4SiSb_2 \rightarrow Ti_4ZBi_2$ (Z = Cr, Mn, Fe, Co, Ni),[8,9] $Nb_4Pd_{0.5}SiSb_2 \rightarrow Nb_4Pd_{0.5}ZSb_2$ (Z = Cr, Fe, Co, Ni), and $Ta_4SiTe_4 \rightarrow Ta_4ZTe_4$ (Z = Cr, Fe, Co, Ni).[15,35] Attempts to synthesize Ta analogues of $Nb_4Pd_{0.5}ZSb_2$ have thus far been unsuccessful.

Electronic Structure. Band structure calculations for both $Nb_4Pd_{0.5}FeSb_2$ and $Nb_4Pd_{0.5}SiSb_2$ were carried out, but as the conclusions are generally similar, we present detailed results for only the former. In these intermetallic compounds where electronegativity differences are small, a bonding description involving full transfer of electrons from one component to another is probably quite unrealistic. By analogy with V_4SiSb_2 or Ti_4FeBi_2,[9] one might begin with an improbable formulation such as "$(Nb^{3+})_4(Pd^0)_{0.5}(Fe^{6-})(Sb^{3-})_2$" for which the main insight would be that substantial metal−metal bonding must arise from the presence of such an electron-rich metal center as Fe^{6-}.

The density of states (DOS) plot for $Nb_4Pd_{0.5}FeSb_2$ is shown in Figure 3. As expected for this metal-rich compound, the Fermi level at −10.08 eV falls in a region of high DOS. The DOS around the Fermi level is dominated by Nb 4d states (Figure 3a). Most of the Pd 4d states are found below the Fermi level

(30) Bradtmöller, S.; Kremer, R. K.; Böttcher, P. *Z. Anorg. Allg. Chem.* **1994**, *620*, 1073.
(31) Villars, P. *Pearson's Handbook, Desk Edition*; ASM International: Materials Park, OH, 1997.
(32) Kwon, Y.-U.; Sevov, S. C.; Corbett, J. D. *Chem. Mater.* **1990**, *2*, 550.
(33) Kleinke, H.; Ruckert, C.; Felser, C. *Eur. J. Inorg. Chem.* **2000**, 315.
(34) Gladyshevskii, E. I.; Kuz′ma, Yu. B. *J. Struct. Chem. (Engl. Transl.)* **1965**, *6*, 60.
(35) (a) Badding, M. E.; Gitzendanner, R. L.; Ziebarth, R. P.; DiSalvo, F. J. *Mater. Res. Bull.* **1994**, *29*, 327. (b) Ahn, K.; Hughbanks, T.; Rathnayaka, K. D. D.; Naugle, D. G. *Chem. Mater.* **1994**, *6*, 418. (c) Neuhausen, J.; Finckh, E. W.; Tremel, W. *Chem. Ber.* **1995**, *128*, 569.

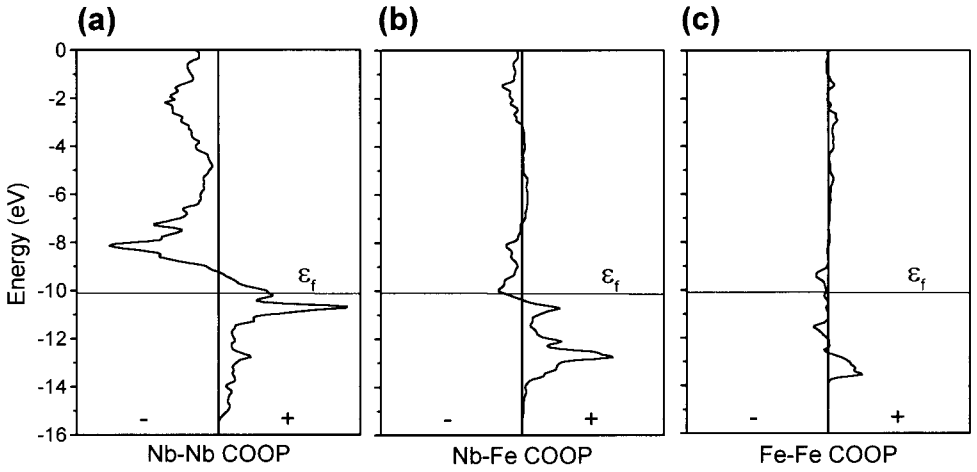

Figure 4. Crystal orbital overlap population (COOP) curves for (a) Nb−Nb, (b) Nb−Fe, and (c) Fe−Fe interactions, within the range of distances listed in Table 3, in $Nb_4Pd_{0.5}FeSb_2$.

(Figure 3b), supporting their crude description above as zero-valent Pd. Although the Fe 3d states are spread over a wide energy range and their contribution at the Fermi level is still substantial (Figure 3c), a large proportion is localized between −11 and −14 eV. The Sb 5p states lie mostly below the Fermi level (and the 5s states are even lower) (Figure 3d).

As in most polar intermetallic compounds, metal−metalloid bonding interactions are strong and optimized in $Nb_4Pd_{0.5}FeSb_2$: the Mulliken overlap population (MOP) is calculated to be 0.31 for the Nb−Sb bonds and 0.26 for the Pd−Sb bonds. However, as the analysis of the DOS above suggests, it is the strength of homo- and heteroatomic metal−metal bonds involving Nb and Fe atoms that will play the key role in determining the stability of the structure. The crystal orbital overlap population (COOP) curves for Nb−Nb, Nb−Fe, and Fe−Fe interactions in $Nb_4Pd_{0.5}FeSb_2$ are plotted in Figure 4. For the Nb−Nb interactions, most bonding levels are occupied, indicating fairly strong Nb−Nb bonding (MOP = 0.19) (Figure 4a). The intercolumn Nb−Nb contact of 3.1448(16) Å is significant (MOP = 0.21), showing that it plays an important role in holding adjacent $^1_\infty[Nb_{8/2}Z]$ columns together. The Nb−Fe bonding interactions are almost optimized with all bonding states and only a small portion of antibonding states being occupied (MOP = 0.24) (Figure 4b). The Fe−Fe COOP curve displays features characteristic of a one-dimensional chain of bonded metal atoms (d_{Fe-Fe} = 2.4772(1) Å) (Figure 4c). Interactions involving $d_{z^2}-d_{z^2}$ σ-overlap result in bonding states around −13 eV, which are occupied, and antibonding states around −9.5 eV, which remain unoccupied. Interactions involving $d_{xz}-d_{xz}$ and $d_{yz}-d_{yz}$ π-overlap give rise to bonding levels near −13 eV and antibonding levels near −11.5 eV, both of which are occupied. The overlap population calculated for the 2.4772(1) Å Fe−Fe contact is 0.13, about one-third of the MOP expected for an Fe−Fe single bond.[10]

The electronic structure of $Nb_4Pd_{0.5}SiSb_2$ resembles that of $Nb_4Pd_{0.5}FeSb_2$, except that, without any contributing d orbitals from the interstitial Si atom, the DOS near the Fermi level is dominated almost entirely by Nb 4d states and the Si−Si bonds must arise from overlap of sp hybrid orbitals. The 2.4817(2) Å Si−Si contact has an MOP of 0.40, also about one-third of the theoretically maximum MOP expected for a Si−Si bond within a chain, and somewhat stronger than the even shorter Si−Si bonds (2.35−2.45 Å) in Ta_4SiTe_4 (MOP = 0.280).[36]

There are some interesting anomalies in the trends in the composition and structure of $Nb_4Pd_{0.5}ZSb_2$ upon substitution with different interstitial atoms Z. The mixing of Si into the interstitial site in $Nb_4Pd_{0.5}Cr_{0.28}Si_{0.72}Sb_2$ is not restricted to Cr; analogous compounds in which Si is mixed with the other transition metals Fe, Co, and Ni can be easily prepared, and indeed improved crystallization is promoted when the reactions are performed in silica tubes! It is likely that the interstitial Z−Z distance of ∼2.48−2.50 Å remains relatively inflexible, a manifestation of a matrix effect imposed by having to satisfy geometrical requirements to optimize Nb−Nb and Nb−Sb bonding in $Nb_4Pd_{0.5}ZSb_2$ foremost, similar to what has been proposed for the short Si−Si bonds in V_4SiSb_2. Although it is difficult to compare strengths of bonds of different types, we suggest that the host structure would then prefer to accommodate the main-group element rather than a transition metal to form stronger Si−Si bonds (involving overlap of s and p orbitals) than metal−metal bonds (involving overlap of d orbitals). The ideal Cr−Cr distance in a hypothetical all-Cr compound may be on the verge of exceeding that accessible by the host structure. The longest Z−Z distance found in structures containing square antiprismatic $^1_\infty[M_{8/2}Z]$ columns without any mixing of Z occurring is ∼2.49 Å. Compounds that are stabilized by differential fractional site occupancy (DFSO) such as $Hf_{10}M_xSb_{6-x}$ have significantly longer Z−Z distances (∼2.8 Å) where Z is a mixture of M and Sb.[33]

Unlike the other members, $Nb_4Pd_{0.5}Ni_{0.78}Sb_2$ is substoichiometric in the Z site. Assuming a rigid band model, the addition of electrons to $Nb_4Pd_{0.5}ZSb_2$ on progressing to the right along the first-row transition metals raises the Fermi level. Although this strengthens Nb−Nb bonding (Figure 4a), it weakens Nb−Z and Z−Z bonding through the occupation of antibonding levels (Figure 4b,c). Correspondingly, the Nb−Ni and Ni−Ni distances are longer than expected in $Nb_4Pd_{0.5}Ni_{0.78}Sb_2$ (Table 3). The predictions are not perfect (the Nb−Nb distances are actually longer), but the occurrence of the Ni substoichiometry represents an alternative to tolerating further bond distortions.

The absence of a Mn-containing member, "$Nb_4Pd_{0.5}MnSb_2$", is curious, but it should be noted that the Nb_4ZTe_4 and Ta_4ZTe_4 series also lack this member.[35] (Trace amounts of Mn (<3%) mixed in with a larger proportion of Si (∼11%) were

(36) Li, J.; Hoffmann, R.; Badding, M. E.; DiSalvo, F. J. *Inorg. Chem.* **1990**, *29*, 3943.

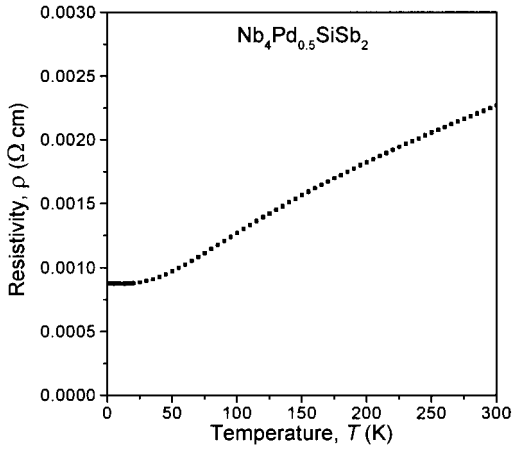

Figure 5. Temperature dependence of the resistivity of a pressed pellet of $Nb_4Pd_{0.5}SiSb_2$.

noted in a few small crystals found in some reactions, but as this is near the detection limit of EDX analysis, the verdict remains unclear.)

As expected from the band structure, $Nb_4Pd_{0.5}SiSb_2$ displays metallic behavior with the resistivity decreasing linearly with decreasing temperature ($\rho_{300} = 2.2 \times 10^{-3}$ Ω cm; $\rho_2 = 0.87 \times 10^{-3}$ Ω cm) until it levels off to its residual value below ~25 K (Figure 5). The absolute resistivities are somewhat high for a metal, probably an effect of grain boundaries present in the pressed pellet sample.

The $Nb_4Pd_{0.5}ZSb_2$ series expands on the rich structural chemistry of the pnictides, showing that cluster-type extended structures need not be limited to the chalcogenides and halides. The insertion of Pd into the V_4SiSb_2-type structure instead of more electropositive atoms such as Li or Na, as proposed previously,[10] is perhaps surprising, but understandable in view of the need to form covalent bonds of low polarity in an intermetallic structure. As illustrated by the wide range of Z atoms that can be substituted in the $Nb_4Pd_{0.5}ZSb_2$ series, interstitial chemistry provides yet another tool in the solid-state chemist's repertoire for imparting stability and flexibility in extended structures.

Acknowledgment. The Natural Sciences and Engineering Research Council of Canada and the University of Alberta supported this work. We thank Christina Barker (Department of Chemical and Materials Engineering) for assistance with the EDX analyses.

Supporting Information Available: An X-ray crystallographic file in CIF format for the structures of $Nb_4Pd_{0.5}ZSb_2$ (Z = Cr, Fe, Co, Ni, Si). This material is available free of charge via the Internet at http://pubs.acs.org.

IC010441Z